

Demonstration of a simplified optical mouse lighting module by integrating the non-Lambertian LED chip and the free-form surface

Jui-Wen Pan^{1,2,3,*} and Sheng-Han Tu⁴

¹Institute of Photonic System, National Chiao Tung University, Tainan 71150, Taiwan

²Biomedical Electronics Translational Research Center, National Chiao Tung University, Hsin-Chu, 30010 Taiwan

³Department of Medical Research, Chi Mei Medical Center, Tainan 71004, Taiwan

⁴Genesis Photonics Inc., No. 5 Dali 3rd Road, Tainan Science-Based Industrial Park, 741, Taiwan

*Corresponding author: juiwenpan@gmail.com

Received 5 December 2011; revised 28 March 2012; accepted 30 March 2012;
posted 2 April 2012 (Doc. ID 159429); published 15 May 2012

A cost-effective, high-throughput, and high-yield method for the efficiency enhancement of an optical mouse lighting module is proposed. We integrated imprinting technology and free-form surface design to obtain a lighting module with high illumination efficiency and uniform intensity distribution. The imprinting technique can increase the light extraction efficiency and modulate the intensity distribution of light-emitting diodes. A modulated light source was utilized to add a compact free-form surface element to create a lighting module with 95% uniformity and 80% optical efficiency. © 2012 Optical Society of America

OCIS codes: 350.3950, 230.3670, 220.4000, 220.2945.

1. Introduction

Recently, GaN light-emitting diodes (LEDs) have attracted plenty of interest due to their favorable characteristics, such as high flux efficiency, reliability, low power consumption, long life, and environmental friendliness [1,2]. These LEDs have already been extensively adopted in several practical applications, for example as backlight light sources for flat panels, in mobile projectors, for street lighting, traffic signals, automotive lighting, and general lighting [1,2]. However, the ratio of refractive index between GaN ($n = 2.5$) and air ($n = 1.0$) is 2.5, which causes considerable photons to be trapped inside the GaN chip due to the total internal reflection (TIR), where they are then absorbed and converted into heat. Fortunately, the external quantum efficiency of GaN-based

LEDs can easily be improved by enhancing the escape probability of the trapper photons. Methods that can increase the external quantum efficiency include reducing the surface roughness [3], utilizing photonic crystals [4], patterning the sapphire substrate [5], and imprinting techniques [6,7]. These methods introduce a relative roughness interface between the air and the LED chip so that the opportunity for photons to escape from inside the GaN chip increases.

Agilent was the first company to develop an optical mouse with an LED light source. The conventional LED mouse optical module included two subparts. One was the image subpart, which consisted of an imaging lens and a complementary metal-oxide semiconductor (CMOS) sensor, and the other the illumination path. The imaging lens constructed a conjugation relationship between the CMOS sensor and the active area. Following the illumination path, the illumination lens would collect the light emitted from

1559-128X/12/152834-08\$15.00/0
© 2012 Optical Society of America

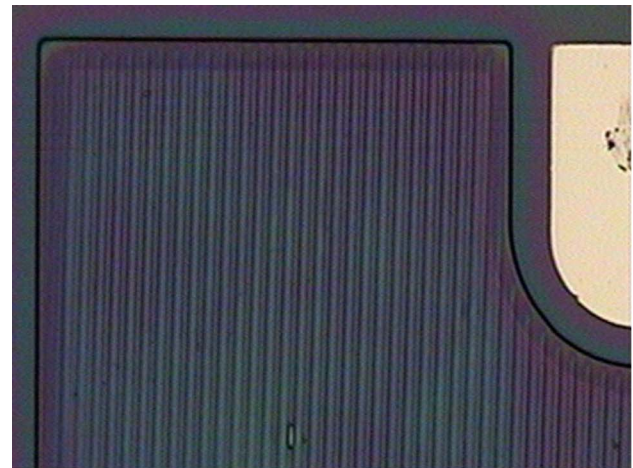
the LED chip, simultaneously homogenizing the distribution of the illumination over the active area. The illumination lens also converted the incident angle of the emitting light so that it impinged on the illuminated area from 17° to 22° for the production of a high-contrast image [8]. In a conventional illumination lens, the double TIR and three exit facets were adopted to produce a homogenized illumination distribution throughout the active area [9]. However, there is decay in the reflection efficiency when the double TIR surface is contaminated by dust or particles. Moreover, the double TIR mechanism limits the angle of ray propagation and reduces the total optical efficiency of the illumination lens to less than the manufacturer's recommended tolerance [10]. Another characteristic of the conventional illumination lens is the un-uniformity on the active area. In a conventional illumination lens, the double TIR condition is utilized to produce a virtual image. The design of the three exit facets ensures that the virtual images are superimposed on the illuminated surface [11]. However, the uniformity produced by the illumination lens is only about 65%; moreover, the three exit facets also produce three hot spots that reduce the illumination uniformity. There is an additional loss of optical efficiency owing to the two hot spots outside the conjugation area of the image sensor. A reduction in the efficiency loss and increase in the uniformity both lead to improved performance of the illumination lens for adoption in the optical mouse.

In this study, we demonstrate a novel method that satisfies both demands for an illumination lens for the optical mouse. The imprinting technique introduced after the chip fabrication process helps to increase the light extraction efficiency of the LED by 14% and modulates the near-field pattern at the chip level to match the peak intensity of 22° needed for optical mouse applications. Furthermore, a corresponding optical element designed for a free-form surface is also integrated with the imprinted LED chip to optimize the illumination of the lens. The uniformity on the illuminated surface was raised to 95% after removal of TIR loss and three hot spots. Most important of all, both the imprinting technique and the free-form illumination lens are cost-effective, having the high throughput, compact size, and high yield needed for mass production. Finally, the novel design for free-form surface illumination was fabricated and tested. All optical performance results were consistent with the optical simulation results. Clearly, the novel illumination system offered improved illumination efficiency and image contrast.

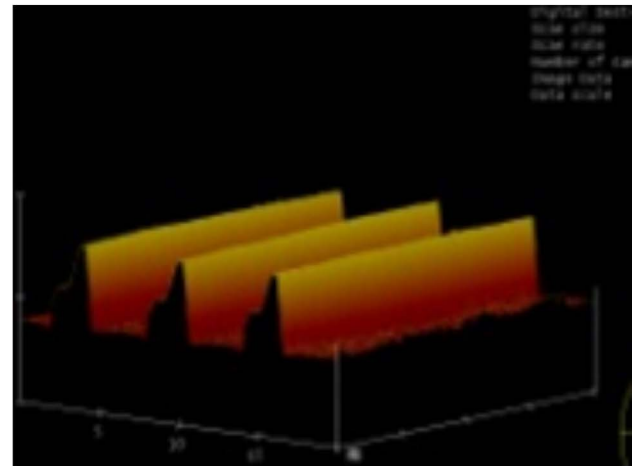
2. Imprinting and Chip Process

The intensity pattern of the planar LED chip has the characteristics of a Lambertian light source: a peak intensity located in a direction normal to the lighting surface, and a half intensity at $\pm 60^\circ$ relative to the normal axis [12]. The structure imprinted on the planar LED chip surface cause a shift in the Lambertian properties.

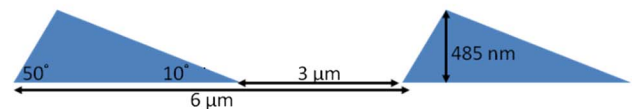
The chip fabrication process included mesa definition and etching, the addition of a transparent conductive layer (TCL) and deposition of the Cr-Au electrode pad [13]. After the chip fabrication process, a Si mold and spin-on-glass (SOG) were used to fabricate a one-dimensional (1D) grating structure on the top of the TCL. The period of this grating structure was $6 \mu\text{m}$ with a filling factor of 0.5, and the height was about 385 nm. Figures 1(a) and 1(b) show the optical microscopic (OM) and atomic force microscopic images of the LED chip with the imprinted structure. The imprinted structure, as depicted in Fig. 1(c), has a serrated profile with an asymmetrically blazed structure. The blazing structure has



(a)



(b)



(c)

Fig. 1. (Color online) Microscopic images and geometric depiction of the imprinted structures: (a) $50\times$ optical microscope picture of the imprinted LED chip; (b) AFM picture of the 1D blazed grating structure; (c) 1D blazed grating geometric scheme.

two different angles, 10° and 50°, between each sidewall and the bottom surface.

3. Electrical and Optical Performances

The results of the electric performance of the imprinted and planar LED chips are shown in Fig. 2. Figure 2(a) shows the applied voltage versus current (*I-V*) curve measured in the probe stage. The forward

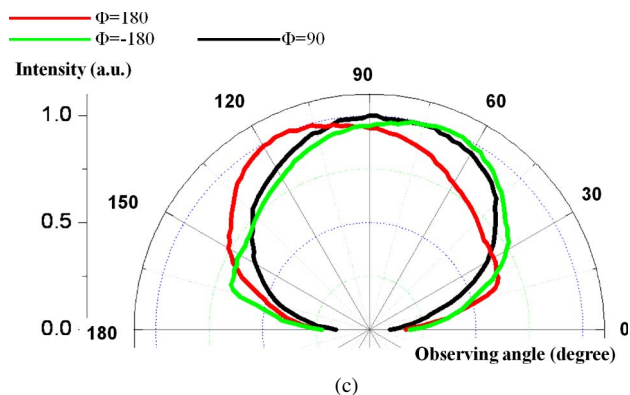
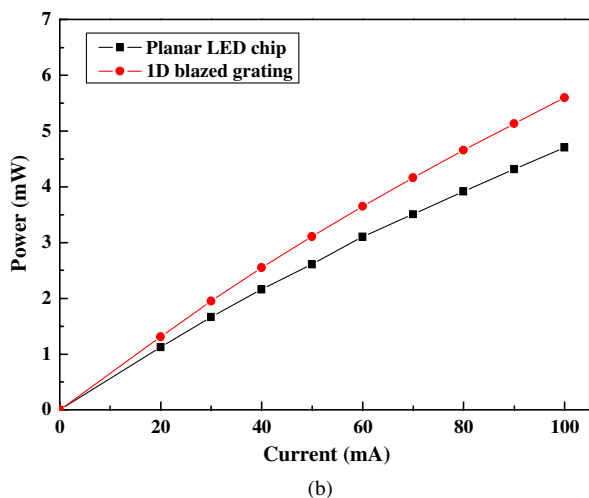
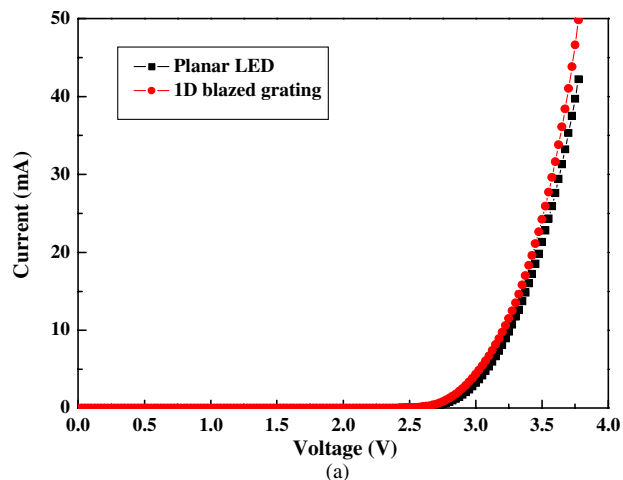


Fig. 2. (Color online) The optical performance of imprinted and planar LEDs: (a) applied voltage versus current curve; (b) injection current versus luminous curve; (c) intensity distributions of imprinted LEDs for 180°, -180°, and 90° measurement.

voltage of the imprinted LED was 3.4 V at a current of 20 mA, similar to that of the planar LED. Although the imprinting process provided a high temperature and pressure environment, the electrical properties of the LED chip were not affected by the imprinting process. Even with an additional pressing and annealing processes, the forward voltage remained at 3.4 V. Figure 2(b) shows the injection current versus output power (*L-I*) curve measured by an integral sphere. Figure 2(b) indicates an enhancement in the output power of 14% for the imprinted LED, compared with that of the planar LED at an input current of 20 mA. The enhancement in the output power was a result of the insertion of medium index material and surface roughness. The indexes were gradually changed effectively by the insertion of an SOG surface texture layer, because the refractive index of the SOG was 1.5. As a consequence, there was a reduction in light trapping from Fresnel loss. The other reason for the light output enhancement was due to the enhancement of escape probability of trapped photons by the imprinted surface texture. Near-field measurement of the LED chip is used to obtain the near-field intensity distribution [14]. Figure 2(c) shows the intensity distribution results from 1D blazed grating LED chips with scanning angles of 180°, -180°, and 90° to the imprinted grating period. The imprinted LED shows a non-Lambertian light with a shift in the peak intensity in both the 180° and -180° scanning direction. Consequently, when the scanning direction is 90°, a Lambertian-like pattern, like that of a planar LED chip, is presented.

4. Optical Design and Simulation

There are many different technologies used in this field for moving sensing applications, especially to meet the specifications for an LED optical mouse [9]. The image contrast is affected by the incident angle between the light source and the illuminated surface. Generally, the best incident angle is around 17° to 22° [8]. A conventional illumination lens has three functions: first, collection of the emitting light; second, homogenization of the light distribution; and third, control of the incident angle in the active area. In this study, the incident angle is controlled by the blazed grating fabricated on the LED chip surface. The illumination lens is designed to enhance the illumination homogenization and the collection efficiency.

In order to attain these two goals, we use a free-form surface (FFS) with compact size. The Advanced System Analysis Program (ASAP) blazer curves are adapted to construct the free-form surface, which can be described as an *m* by *n* tensor product $P(u, v)$, as shown in Eq. 1 [15].

$$P(u, v) = \frac{\sum_{i=0}^m \sum_{j=0}^n P_{ij} W_{ij} B_i^m(u) B_j^n(v)}{\sum_{i=0}^m \sum_{j=0}^n W_{ij} B_i^m(u) B_j^n(v)}, \quad (1)$$

where P_{ij} , W_{ij} is a set of $(m + 1)(n + 1)$ control points and weight factors; $B_i^m(u) = \frac{(1-u)^{m-1} u^i m!}{i!(m-i)!}$ is the

Bernstein polynomial; and each control point has three values, x, y, z , in the Cartesian coordinate system. The $(m + 1)(n + 1)$ control points and weight factors are used to control the surface normal vector of each local unit surface of the free-form surface. Then we can modulate the local ray impinging on the local unit surface of the free-form surface to the active area on the illumination surface.

In order to obtain the two aforementioned goals, two kinds of FFSs are used to homogenize the illumination distribution and collect the emitted light [16,17]. They are shown in Fig. 3. The radiation pattern from the LED chip with the imprinted microstructure can be divided into two regions by the optical axis. In our system, the optical axis is set as the z global axis. One region is under the optical axis with the peak intensity, and the other is above the optical axis. The four FFSs can also be divided into two parts. One part has two green surfaces for

collecting the intensity distribution underneath the optical axis and homogenizing the illumination distribution on the target area. The two green surfaces are symmetrical with the z - x plane owing to the 1D blazed grating. The green surface consists of 7×13 control points and weight factors for $m = 6$ and $n = 12$. The other part is marked by two red surfaces for collecting the light above the optical axis and homogenizing the illumination distribution on the illuminated area. The two red surfaces are also symmetrical with the z - x plane owing to the 1D blazed grating. The red surface consists of 7×13 control points and weight factors for $m = 6$ and $n = 12$. The green and red FFSs with control points for the two regions are shown in Figs. 3(a) and 3(b).

Owing to the division of the illumination system into two FFSs, there are also two optical paths. Along the first optical path, the emitting ray passes through the green surface and then impinges on the active area. The rays coming from the first optical path comprise the main intensity controlled by blazed grating. First, the merit function is used to calculate 7×13 control points and 7×13 weight factors for the green surface with uniformity and the peak intensity angle. The green surface is the common surface for the two optical paths; thus, we designed this surface first. After finishing the green surface, the other surface was designed. The other free-form surface controls only the second optical path, which is comprised of emitted rays collected by the red surface, then passing through green surface, until finally impinging on the active area. In the second step, the 7×13 control points and 7×13 weight factors of the red surface are also calculated. Two sets of control points and weight factors are used in the merit function to modulate the green and red FFSs to control the emitted light. The merit functions adopted in this paper are the uniformity and the peak intensity at 22° on the illuminated surface ($1 \text{ mm} \times 1 \text{ mm}$ active area with black rectangle) as follows: For the peak intensity in the active area:

$$T_{\max}(\theta) \sim \text{maximum}, \quad (2)$$

when $\theta = 22^\circ$. For uniformity in the active area (1 mm^2 area):

$$\text{Uniformity} = \frac{I_{\text{cen}}}{I_{\text{avg}}} \times 100\%. \quad (3)$$

For the total optical efficiency:

$$E = \frac{\sum_{p,q} I_{p,q} \times A_{p,q}}{W_{\text{total}}} \times 100\%. \quad (4)$$

For the angle space at the active area, we obtained the intensity distribution function of $T(\theta)$, so as to find the peak intensity $T_{\max}(\theta)$. The merit function was used to control the two sets of control points and the weight factors to locate the peak intensity at 22° in the active area. In other words, the peak

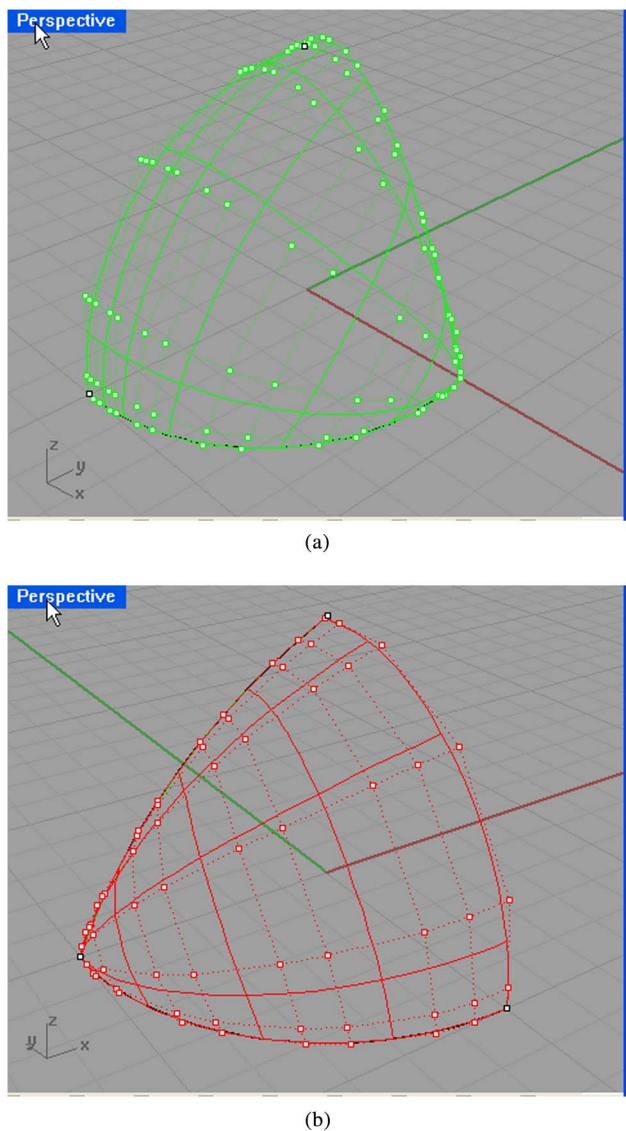


Fig. 3. (Color online) Free-form surface with control points: (a) green surface; (b) red surface.

intensity was 68° with the surface normal of the active area. To find the spatial intensity distribution over the active area, we divided the active area into a p by q mesh with both p and q being integers. Each mesh had local irradiance $I_{p,q}$. The I_{cen} is the irradiance of the mesh at the center of the active area; the I_{ave} is the average irradiance at the active area. W_{total} is the total power emitted from the LED chip.

The optimization process is divided into three main steps. In the first step, we try to simplify the LED source by using point source. The angle distribution of the point source is apodized by the distribution function shown in Fig. 2(c). By using this simple light source, we can calculate the start point and end point for each local unit surface of green surface. After the first step, we calculate only the start point and end point for the free-form surface. The

control point is set at the middle of the start point and the end point for each local unit surface. The weight factor is 1 for all local unit surfaces. With the optimization condition at this step, we only use Eq. (2) to get the correct angle distribution and the peak intensity angle.

In the second step, we try to add eight point sources with apodization at the x - y plane by three times. The first time, we add the two points at $(0.1, 0)$ and $(-0.1, 0)$, then do the optimization process with only the start point and end point for each local unit surface. The second time, we add the two points at $(0, 0.1)$ and $(0, -0.1)$ then do the optimization process with only the start point and end point for each local unit surface. The final time, we add the four points at $(0.1, 0.1)$, $(-0.1, 0.1)$, $(-0.1, -0.1)$, and $(0.1, -0.1)$ and then do the optimization process with

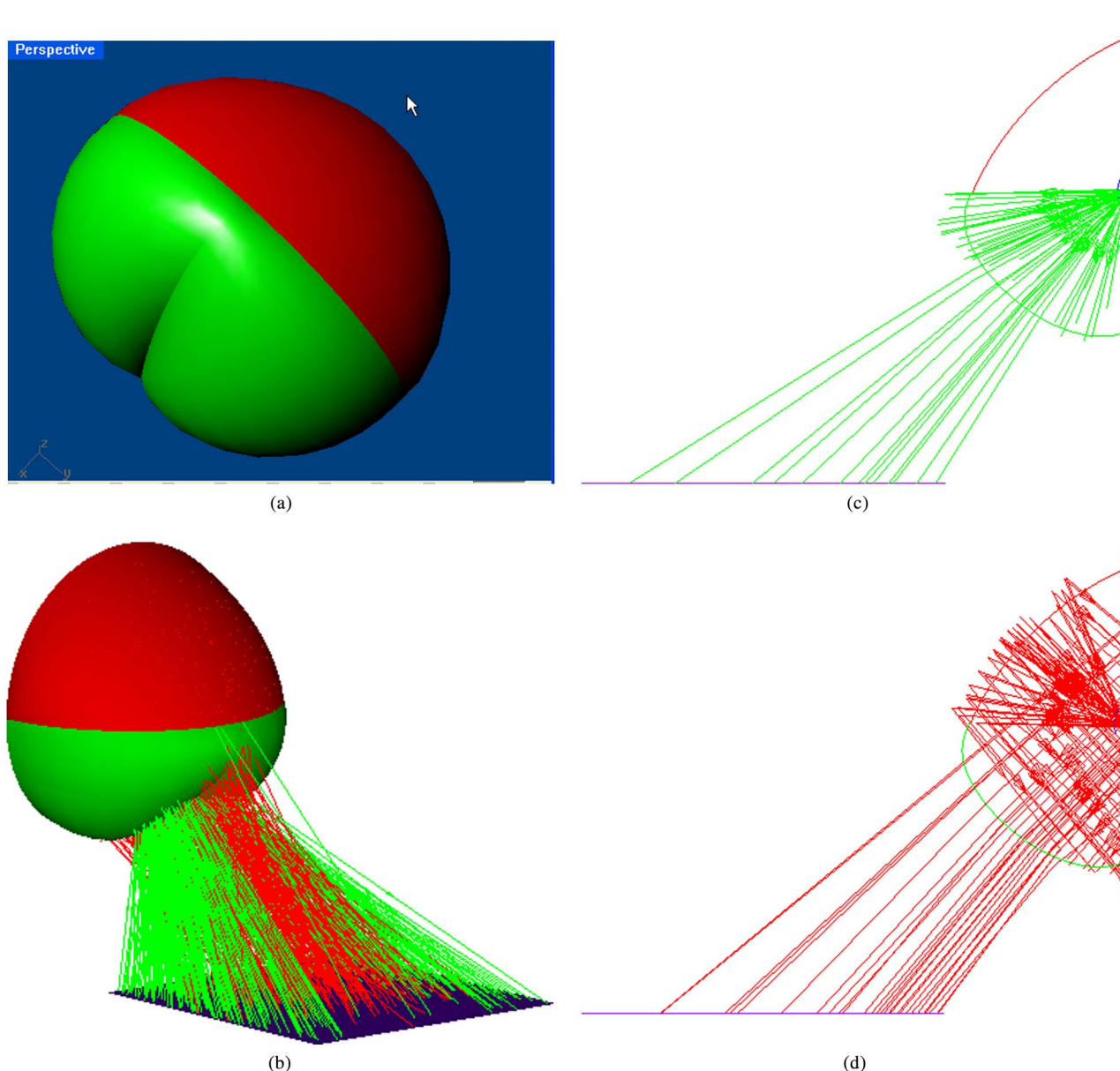
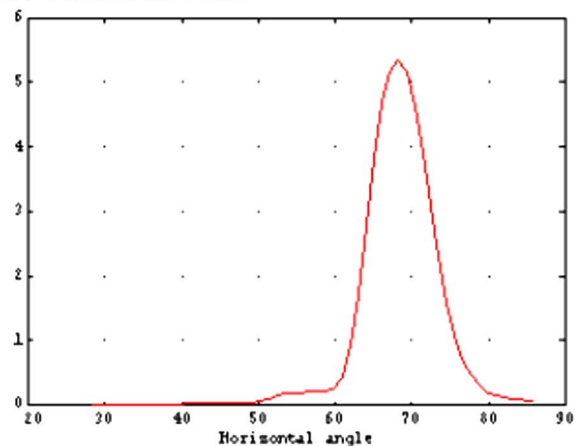


Fig. 4. (Color online) The FFS LED lens: (a) oblique view; (b) ray tracing; (c) green ray path; (d) red ray path in x - z cross section.

MCUODL FINAL RESULT

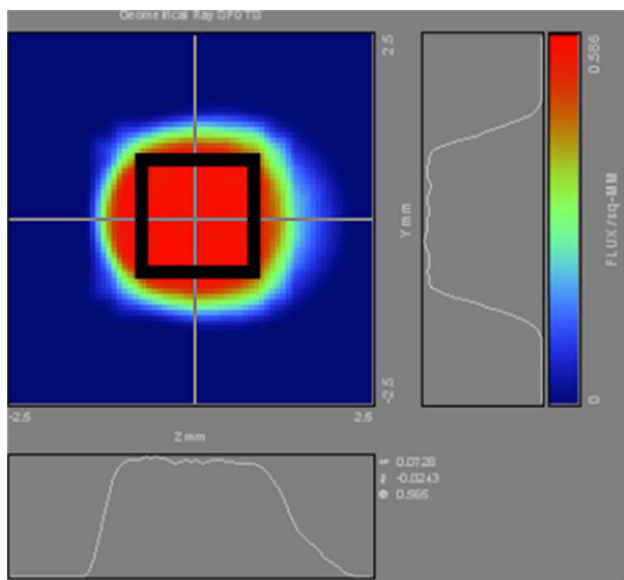
FLUX / STERADIAN for $\lambda = 2785$



ASAP Pro v7.5.0

2010-10-20 10:07

(a)



(b)

Fig. 5. (Color online) Radiant intensity distribution and energy distribution of the illumination distribution with the active area.

Table 1. Comparison of the Traditional and Novel Illumination System

Illumination system	Conventional illumination system [9] (light pipe and three facets at exit port)		Four FFS system (four FFSs)
	Optical Efficiency	Uniformity	
Optical Efficiency	40%	80%	80%
Uniformity	65%	95%	95%
Alignment method	Horizontal	Horizontal	Horizontal
Size (mm ³)	16 mm ³	4 mm ³	4 mm ³
Total internal reflection	2	0	0

only start point and end point for each local unit surface. With the optimization condition, we use Eqs. (2–4) to get the correct angle distribution and uniformity distribution with high efficiency.

In the third step, we try to use the extended light source (0.2 mm × 0.2 mm) with apodization to replace the night point sources. We still optimize the start point and end point once again. Then we use the control point and weight factor to do the optimization and freeze all parameters of the start point and end point of all local unit surfaces. Finally all parameters, including start point, end point, control point, and weight factor, were used to do the optimization with feedback function for uniformity. The feedback times are eight in optimization code [18].

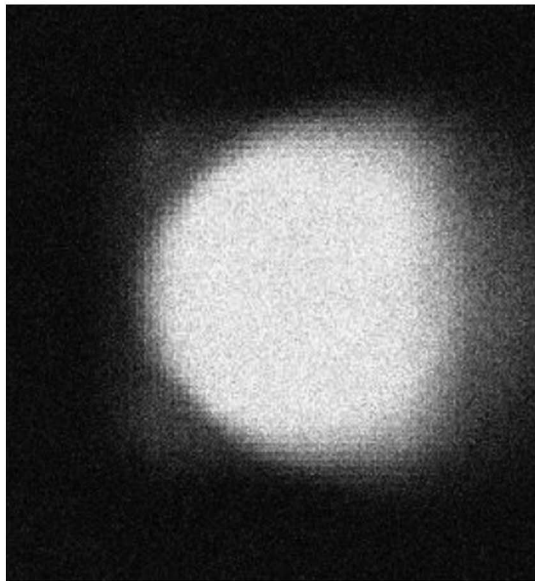
The final optimization results for the four FFSs are shown in Fig 4(a). A representation of the ray tracing of the four FFSs is shown in Figs. 4(b), 4(c), and 4(d). The energy distribution and radiant intensity distribution at the illuminated surface are shown in Fig 5. The incident angle at the peak intensity is 68° with the normal vector of the illuminated surface. A high-contrast image is obtained with the image lens with this incident angle [8]. The uniformity at the active area (1 mm × 1 mm active area with back rectangle) is 95%. The optical efficiency is 80%. The results of a comparison of our design with the conventional design are shown in Table 1. An examination of the table shows that we get better performance in terms of optical efficiency, uniformity, and compact size with our device. The tolerance is the key manufacturing issue for optical systems. We also compared the two systems for LED misalignment issues for mass

Table 2. Comparison of Given Alignment Tolerance for the Two Illumination Systems

Misalignment of LED		Conventional illumination system [9]		Four FFS system	
		Optical efficiency	Uniformity	Optical efficiency	Uniformity
Decenter along x-axis*	+0.05 mm	36%	63%	75%	89%
	-0.05 mm	35%	64%	73%	90%
Decenter along y-axis	+0.05 mm	36%	64%	73%	89%
	-0.05 mm	37%	63%	74%	90%
Decenter along z-axis	+0.05 mm	38%	64%	78%	91%
	-0.05 mm	40%	65%	77%	90%
Rotation around x-axis**	+2°	34%	61%	73%	88%
	-2°	35%	60%	72%	87%
Rotation around y-axis	+2°	33%	62%	71%	89%
	-2°	34%	61%	73%	86%



(a)



(b)

Fig. 6. (a) FFS lens sample; (b) illumination pattern captured by camera.

production. The results are shown in Table 2. The optical efficiency and uniformity of our design was better than that of the traditional design. We proposed a highly efficient and compact volume optical motion sensor. Even under the worst alignment conditions, the optical performance of our device was better than that of the conventional system. Finally, a working sample of the novel free-form surface lens was finished, as shown in Fig. 6(a). An optical mouse was assembled as well. A CMOS camera was used to capture the illumination distribution. The illumination distribution is shown in Fig. 6(b). The simulation results for the illumination distribution are consistent with the CMOS picture. The CMOS sensor intensity showed the intensity to be enhanced 1.9 times over that of the conventional illumination system. The result is also similar to the tolerance analysis. In a word, the novel free surface system is better than the traditional illumination system.

5. Conclusions

In this study we applied a cost-effective, high-throughput, and high-yield imprinting technique for fabrication of an LED chip. The imprinted layer not only increased the light extraction efficiency of the LED chip by 14%, but also modulated the far-field pattern on the chip level. A tilted intensity distribution was achieved by using this imprinted layer. Furthermore, the corresponding free-form surfaces were designed for an optical mouse application. The uniformity at the illuminated surface was 95%. The optical efficiency was 80%. The characteristics of the four free-form surfaces included the compact size, low fabrication cost, and the total internal reflection loss was excluded in our lighting module. The imprinted LED and optical element design are integrated to obtain an illumination system with a higher optical efficiency, more uniform intensity distribution, and more compact size. Finally, a sample of the novel free-form surface illumination system was finished and tested. The test results show a performance very similar to the simulation results.

This study was supported in part by the National Science Council, project number NSC100-2220-E-009-023 and NSC101-2314-B-384-001, and in part by the "Aim for the Top University Plan" of the National Chiao Tung University and Ministry of Education, Taiwan, Republic of China.

References

1. E. F. Schubert and J. K. Kim, "Solid-state light sources getting smart," *Science* **308**, 1274–1278 (2005).
2. M. S. Zukauskas, M. S. Schur, and R. Gaska, *Introduction to Solid State Lighting* (Wiley-Interscience 2002).
3. T. Fuji, "Increase in the extraction efficiency of GaN-based light-emitting diodes via surface roughening," *Appl. Phys. Lett.* **84**, 855 (2004).
4. K. Orita, "High-extraction-efficiency blue light-emitting diode using extended-pitch photonic crystal," *Jpn. J. Appl. Phys.* **43**, 5809–5813 (2004).
5. M. Khizar, Z. Y. Fan, K. H. Kim, J. Y. Lin, and H. X. Jiang, "Nitride deep-ultraviolet light-emitting diodes with microlens array," *Appl. Phys. Lett.* **86**, 173504 (2005).
6. Z. M. Wang, X. J. Lio, S. Wang, C. X. Lio, M. H. Sun, K. Bao, B. Zhang, G. Y. Zhang, Y. G. Wang, Y. Chen, H. Ji, and Q. Ouyang, "Light output enhancement of a GaN-based light emitting diode by polymer film imprinting," *Semicond. Sci. Tech.* **22**, 279 (2007).
7. K. Bao, X. N. Kang, B. Zhang, T. Dai, C. Xiong, H. Ji, G. Y. Zhang, and Yong Chen, "Improvement of light extraction from patterned polymer encapsulated GaN-based flip-chip light emitting diodes by imprinting," *IEEE Photon. Tech. Lett.* **19**, 1840–1842 (2007).
8. B. J. Tullis, "Method and device for achieving high contrast surface illumination," U.S. patent 5686720, (11 November, 1997).
9. Avago (Agilent), "HDNS-2100 solid-state optical mouse lens data sheet," <http://www.avagotech.com.tw/docs/AV02-1278EN>.
10. R. E. Fisher and B. Tadic-Galeb, *Optical System Design* (McGraw-Hill, 2000).
11. G. E. Smith, "Illumination optics and method," U.S. patent 6476970, (5 November, 2003).
12. E. F. Schubert, "The Lambertian emission pattern," in *Light-Emitting Diodes* (Cambridge University, 2006), pp. 94–95.
13. S. H. Tu, S. Y. Wu, Y. C. Lee, J. W. Pan, C. H. Kuo, C. M. Wang, and J. Y. Chang, "Functional imprinting structures on GaN-based light-emitting diodes for light pattern modulation

- and light extraction efficiency enhancement,” *Opt. Rev.* **17**, 379–384 (2010).
14. Radiant Zemax, “SIG-400TM,” <http://www.radiantimaging.com/index.php?q=products/sig400>.
 15. “Advanced System Analysis Program technical guide,” Edges in ASAP, <http://www.breault.com/k-base.php?kbaseID=29&catID=44&page=2>.
 16. J. W. Pan, S. H. Tu, C. M. Wang, and J. Y. Chang, “High efficiency pocket-size projector with a projecting lens and light emitting diode-based light source system,” *Appl. Opt.* **19**, 3406–3414 (2008).
 17. J. W. Pan, S. H. Tu, W. S. Sun, C. M. Wang, and J. Y. Chang, “Integration of non-Lambertian LED and reflective optical element as efficient street lamp,” *Opt. Express* **18**, A221–A230 (2010).
 18. Y. Luo, Z. Fang, Y. Han, and H. Li, “Design of compact and smooth free-form optical system with uniform luminance for LED light source,” *Opt. Express* **18**, 9055–9063 (2010).